JAAS

Accepted Manuscript

This is an *Accepted Manuscript*, which has been through the Royal Society of Chemistry peer review process and has been accepted for publication.

Accepted Manuscripts are published online shortly after acceptance, before technical editing, formatting and proof reading. Using this free service, authors can make their results available to the community, in citable form, before we publish the edited article. We will replace this *Accepted Manuscript* with the edited and formatted *Advance Article* as soon as it is available.

You can find more information about *Accepted Manuscripts* in the Information for Authors.

Please note that technical editing may introduce minor changes to the text and/or graphics, which may alter content. The journal's standard Terms & Conditions and the Ethical guidelines still apply. In no event shall the Royal Society of Chemistry be held responsible for any errors or omissions in this *Accepted Manuscript* or any consequences arising from the use of any information it contains.

ROYAL SOCIETY OF CHEMISTRY

www.rsc.org/jaas

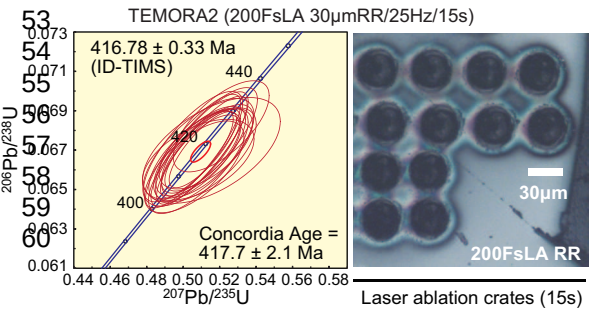

High precision U-Pb dating using multiple Faraday collectors has become available in LA-MC-ICP-MS

TECHNICAL NOTE

An improved U-Pb age dating method for zircon and monazite using 200/266 nm femtosecond laser ablation and enhanced sensitivity multiple-Faraday collector inductively-coupled plasma mass spectrometry†

Jun-Ichi Kimura*[a], Chang Qing[a], Keita Itano[b], Tsuyoshi Iizuka[b], Bogdan Stefanov Vaglarov[a], and Kenichiro Tani[c]

We present an improved U-Pb age dating method for zircon and monazite crystals using 193 nm excimer laser ablation and 200/266 nm femtosecond laser ablation (200/266FsLA) multiple-Faraday collector inductively coupled plasma-mass spectrometry (MFC-ICP-MS). Optimization of the 266 fs laser beam enabled an analysis of $^{207}Pb/^{206}Pb$ and $^{206}Pb/^{238}U$ ratios with an in-run precision of 1–2% from a crater of dimensions 50 μm×10 μm (diameter × depth) at a repetition rate of 2 Hz for 30 s. The same in-run precision was obtained from a 30 μm×20 μm crater using a 200 fs laser beam 20 μm in diameter rastered along the circumference of a circle with a 7 μm radius at 25 Hz for 15 s. With an enhanced sensitivity ion interface, the sensitivity for the total amount of Pb was ~2 mV/ppm or ~125,000 cps/ppm using the above crater setup. The use of high gain amplifiers equipped with a 10^{12} Ω register enabled a determination of the U-Pb age of zircon and monazite crystals with internal and intermediate precision comparable to that obtained from sensitive high resolution ion microprobe (SHRMP) techniques. We analysed standard zircon crystals using a 91500 zircon (1065.4 ± 0.6 Ma determined by isotope dilution thermal ionization mass

spectrometry (ID-TIMS)) as a bracketing standard. Ages determined from TEMORA2, Prešovice, and OD-3 zircons compared very well with their reference ages determined by ID-TIMS and/or SHRIMP. Thompson Mine and Monangotory standard monazites, dated using a 44069 monazite (424.9 ± 0.4 by ID-TIMS) as a standard, also reproduced the U-Pb ages determined by ID-TIMS/LA-MFC-ICP-MS, but at a sample volume four times smaller than that required for zircons. Zircon and monazite ages are accurate given the small offsets from ID-TIMS ages, 0.15–0.7% for zircons and 0.2–0.7% for monazite well within internal precision from the primary standard in the analytical session and competitive with internal precision of 0.43–0.6% for zircon and 0.2–0.8% for monazite. More easily obtaining high resolution age data is useful for the precise determination of U-Pb age.

[a] Department of Solid Earth Geochemistry (DSEG), Japan Agency for Marine-Earth Science and Technology (JAMSTEC), 2-15 Natsushima-Cho, Yokosuka 237-0061, Japan.

[b] Department of Earth and Planetary Science, University of Tokyo, Hongo 7-3-1, Bunkyo, Tokyo 113-0033, Japan

[c] Division of Mineral Sciences, National Museum of Nature and Science, Amakubo 4-1-1, Tsukuba, Ibaraki 305-0005, Japan

E-mail: jkimura@jamstec.go.jp; Fax: +81-46-867-9625; Tel: +81-46-867-9765

† Electronic supplementary information (ESI) available: Data Table 1: Analytical results of U-Pb age. See DOI:10.1039/c4jaxxxxxg

1. Introduction

U-Pb dating of zircon crystals using in-situ laser ablation inductively coupled plasma mass spectrometry (LA-ICP-MS) became practical in the mid-1990s through the introduction of ultraviolet (266 nm) yttrium aluminium garnet (YAG) lasers and a high sensitivity ion sampling interface using a quadrupole ICP-MS.[1] This method has become a standard tool in geochronology due to developments in instrumentation and data correction methods.[2-5] However, the intermediate precision for the U-Pb age that can be achieved with this method is still inferior to that of sensitive high resolution ion microprobe (SHRIMP) techniques.[2, 6-8] The ICP-MS technique is inferior to SHRIMP mainly from (1) elemental fractionation between U and Pb during laser ablation,[2, 7, 9-15] or in the ICP plasma,[9, 16, 17] (2) flicker noise in the ICP,[2, 18] and (3) the non-linear response of the ion counter(s).[6, 10, 13, 19, 20]

Elemental fractionation during laser ablation (referred to as downhole fractionation) has been examined intensively. Correction methods for downhole elemental fractionation have been examined.[2, 15, 21] However, a reasonable solution requires further development of laser ablation (LA) systems, a central subject over the past two decades. Use of shorter wavelengths to the deep ultraviolet (DUV) (266 nm, 213 nm, 200 nm, 193 nm, and 157 nm)[4, 12, 22] and the use of ultra-short pulses in the near infrared (NIR: 800 nm) to UV–DUV (~266 and ~200 nm) femtosecond lasers have been investigated.[9, 23-26] As the result, the latest LA systems commonly use UV, a 213–193 nm nanosecond YAG, a 193 nm nanosecond excimer, or a 266–200 nm femtosecond laser. With these lasers, significant minimization of downhole fractionation has been achieved. Such fractionation still occurs, particularly in samples with a refractory matrix (e.g., zircon and monazite).[9, 10, 26-28] Moreover, matrix dependent

element fractionation in the ICP was recognized and examined seriously along with the fractionation at the ablation site. These studies are difficult to interpret because of the interrelation of fractionation processes via ablation–coalescence (LA site) and dissociation (ICP) processes of the laser aerosol particles.[9, 16, 17, 26, 29-32] With this background, the optimization of laser ablation conditions is still necessary even with the latest UV femtosecond LA (FsLA) systems.

Plasma flicker is inevitable in ICP ion sources because the plasma lights in Ar gas flow at atmospheric pressure in response to radiofrequency (RF) energy sources. The kinematic vibrations of the plasma support gas or the applied RF signal lead to flicker.[18] In particular, single ion counters with a peak jumping mode in the ICP-MS suffer directly from this problem. The achievable in-run precision in isotope ratio is as good as ~1% of 1-standard deviation (1SD) and usually 3–5% 1SD for an isotope pair with the isotope ratio departing largely from unity.[2, 3, 5, 14] The fundamental solution of this problem is to use the simultaneous detection of the isotopes of interest by multiple ion detectors either by ion counters or by Faraday collectors.[33, 34] Several manufacturers now provide multiple ion counters (MICs) because signal intensities of the U-Pb isotope measurements usually range from <1000 counts per second (cps) to > 800,000 cps in U-Pb dating. The achievable precision with these MIC systems is as good as ~0.5% 1SD, which rivals the precision of ~0.3–0.4% 1SD by SHRIMP at high ion intensities.[10, 13, 35]

The use of multiple ion counters (MICs) requires a rather complex calibration procedure including the frequent adjustment of (1) dead time correction factors and (2) the non-linear response between ion counters. These factors prevent the use of mass bias corrections in MC-ICP-MS, which is a standard procedure for Faraday collectors.[36-38]

The standard bracketing method can solve these issues for both inter-IC and mass bias fractionations, but careful adjustment of ion beam intensities between samples and standards is required for a good correction due to the non-linear response of individual ion counters.[10, 13, 35, 39] Large ion counters are unable to completely reduce this problem.[20, 40, 41]

The use of multiple Faraday collectors (MFC) provides a potential solution for flicker noise and unstable detectors. Linearity of the MFC is superior by over five to six orders of magnitude (few μV to few V range).[19, 20] Internal correction for mass fractionation can be made nearly perfectly as exemplified by applications in Sr, Nd and Hf isotope analyses using solution or LA-MFC-ICP-MS.[42-44] Standard bracketing is also far easier for MFC because of the stable and linear response.[19, 20] Elemental fractionation is still a problem because this is caused at the laser ablation site[27, 28] and in the ICP.[9, 17] Fractionation is common for U-Pb dating in general for LA-ICP-MS. The use of a matrix matched standard can minimize or even eliminate these problems.[2, 15, 21]

In spite of these advantages in MFC, the improvement of instrumental sensitivity continues to be a major challenge. The sensitivity of a Faraday collector system is about 100 times inferior to that of ion counters.[36, 37] The application of MFC-ICP-MS to U-Pb dating has been made but is limited to minerals with high-U content, such as monazite.[45] The recent progress of MFC-ICP-MS has dramatically increased sensitivity by modification at the ion sampling interface. The development of high transmission sampler and skimmer cones and a high vacuum (<1.8 mbar) applied at the expansion chamber between the two cones increased the sensitivity ~10 times.[46] The use of a high gain Faraday amplifier with a 10^{12} Ω or a 10^{13} Ω resistor increased gain to ~10–100 times with an increase in signal to noise (S/N) ratio by a factor of ~2–

5.[36-38] The properties of the high gain amplifiers have been reported in the previous works using TIMS.[36-38] These developments opened the possibility of using MFC-ICP-MS in U-Pb age determination of zircon and monazite. The combined application of a high transmission interface and a high gain amplifier has been limited to small isotopes such as ^{204}Pb in LA-MFC-ICP-MS[19] or small isotope signals in Os isotope analyses in sparging-MFC-ICP-MS.[38]

The goal of this paper is (1) to evaluate in-run and intermediate precision in U-Pb age dating by 200/266 nm FsLA coupled with enhanced sensitivity MFC-ICP-MS using 10^{12} Ω amplifiers and (2) to demonstrate the versatility of this new technique. We apply this technique to determine U-Pb ages of standard zircon crystals of TEMORA2 (416.78 ± 0.33 Ma),[6, 47] Prešovice (337.13 ± 0.37 Ma),[48] and OD-3 (33.0 ± 0.1 Ma)[8] using a zircon standard of 91500 (1065.4 ± 0.6 Ma).[49] We also determine U-Pb ages of monazite standards of Thompson Mine (1766 Ma)[50, 51] and Monangotry (555 ± 1.8 Ma)[45, 52] using a monazite standard of 44069 (424.9 ± 0.4 Ma).[53] For these samples, we revisited downhole fractionation observed with the 200/266nm FsLA and examined the matrix effect between standards and samples for optimization of ablation protocols.

2. Experimental

2.1. Samples

We analysed standard zircon crystals of 91500,[49] TEMORA2,[6, 47] Prešovice,[48] and OD-3.[8] The Monazite standard crystals were Thompson Mine,[50, 51] Marangotry,[45, 52] and 44069.[53] These crystals were mounted in epoxy and polished to expose the internal surface for analysis. We used 91500 zircon[49] and 44069 monazite[53] as standards. A

NIST SRM610 glass[54] was also analysed as a standard in order to evaluate the matrix effect between the silica-rich synthetic glass and the 91500 zircon.

2.2. Instruments and settings

2.2.1. Laser ablation

We used a 200/266nm femtosecond LA (200/266FsLA) system (OK-Fs2000K, OK Laboratory, Tokyo, Japan) at the Department of Solid Earth Geochemistry, Japan Agency for Marine-Earth Science and Technology (DSEG/JAMSTEC).[9] The 200/266FsLA system uses a Solstice one-box Ti-sapphire femtosecond regenerative amplifier (Spectra-Physics, Santa Clara, CA, USA) with TP-1A THG and TP-1A FHG frequency tripling and quadrupling harmonic generators (Spectra-Physics, Santa Clara, CA, USA). Two objective lenses made of either excimer laser-grade high power fused silica (266 nm) or fluorite (200 nm) were used to focus the beam on the sample surfaces. The resulting craters were 30 μm and 90 μm in diameter for 200 nm and 266 nm at the maximum sizes, respectively. The laser fluence on the sample surface was ~6 J cm^{-2} in 200 nm and ~12 J cm^{-2} in 266 nm modes.[9]

We used 30 μm/2–10 Hz (15 s) and 50 μm/2–4 Hz (30 s) craters in the 266 nm mode by applying apertures with different diameters. A rotation raster ablation protocol[9] was also tested using a 200 nm mode with a 20 μm/5–25 Hz laser beam rastered along a circumference of a circle with a 7 μm radius at velocity of 7 μm s^{-1}, which resulted in a 30 μm crater (15 s). Along with those analyses, a nanosecond 193 nm excimer (193 Ex) LA system (OK-ExLA2000, OK Laboratory, Tokyo, Japan)[9] was also applied for comparison with the laser fluence on the sample surface at ~6 J cm^{-2}, crater diameter 50

μm, with repetition rate 2–3 Hz (30 s). For detailed descriptions of instruments and settings, see **Table 1**.

Helium (~1.2 L/min) was used as the ablation gas.[3, 14] Although some reports suggest He has no effect on element sensitivity,[15] we confirmed that He gas reduced the surface deposition of ablated particles significantly. This indicated better sample transport with less element fractionation, and as a result He gas was used for ablation in all our experiments.[3, 14] He gas after the ablation cell was mixed with Ar sample gas (~1.3 L/min) in a cylindrical mixing chamber with a 70 cm^3 inner volume immediately before reaching the ICP torch.[55] The pulsed signals at low laser repetition rate were sufficiently smoothed out and the washout time to the gas blank level using this mixing device was about 20 s, short enough for normal operations.[10, 42] Pre-ablation of the sample surface at the ablation spot was made for 2 s just prior to ablation for all analytical conditions in order to remove surface contamination of Pb and any aerosol deposits ablated in the previous analyses.

2.2.2. MFC-ICP-MS

The 200/266FsLA or the 193ExLA was coupled to a modified Neptune multiple-Faraday-collector (MFC)-ICP-MS (Thermo Fisher Scientific, Bremen, Germany) at DSEG/JAMSTEC. The MFC-ICP-MS interface was modified by the addition of a high efficiency rotary pump[42] for a high transmission. The JET sampler and X-skimmer cones were used along with the guard electrode (GE) turned on to achieve the best instrument sensitivity (~3000 V ppm^{-1} or ~187.5 Gcps ppm^{-1} Pb in solution mode using an Aridus II desolvating nebuliser).[19, 38] This sensitivity is about 30 times better than the first application of LA-MFC-ICP-MS to the U-Pb dating of monazite, which used ~100

V ppm^{-1} or 6.24 Gcps ppm^{-1}.[45]

Oxide molecular yield under the high sensitivity setup was monitored by the $^{238}U^{16}O^{+}/^{238}U^{+}$ ratio, which was very high at 30–50%. Oxide yield decreases to ~1 % by adjusting (reducing) sample gas flow, but this reduces sensitivity by one tenth. This high oxide yield is a trade-off of the highest sensitivity setting. Previous reports indicated that such the extreme setting should not be used in order to avoid non-mass dependent isotopic fractionation[42, 56, 57] and spectral interference of oxide ions.[43] However, we used this setup because there were no serious interference effects from oxide ions on U and Pb isotopes. The elemental sensitivity of Pb^{+} and U^{+} ions changes with a change in oxide yield because UO^{+} is more effectively formed than PbO^{+} due to the difference in oxide-dissociation energy, which is higher for U = 749 kJ mol^{-1} relative to Pb = 397 kJ mol^{-1}.[58] The additional effect of non-mass dependent fractionation has never been reported in Pb isotopes and may be negligible. However, mass fractionation must be corrected for by the standard bracketing method.[6, 10, 13, 19, 20, 41] In reality, both the elemental sensitivity and the mass bias change with time after the plasma is on, so that frequent standard-sample bracketing was required for this application (see **section** 3.3).

The configuration of the Faraday collectors and Faraday amplifiers is given in **Table 1** along with other instrumental settings. Five high gain amplifiers using a 10^{12} Ω resistor[36] were assigned to the five target isotopes of ^{238}U, and ^{204}Pb, ^{206}Pb, ^{207}Pb, ^{208}Pb whereas a 10^{11} Ω resistor was always assigned to ^{232}Th and specifically assigned to ^{232}Th in monazite analysis because of the high ion current at >1.0 V during the analysis (**Table 1**). Gain calibration was performed daily by applying 3.33 V before any sample analysis. On-peak background baselines were measured twice for 30 s prior to signal acquisition in each analytical run. This measurement eliminated any cone memories and

gas blanks including ^{204}Hg interference on ^{204}Pb.[19] The ^{204}Pb signal was not used in this study, but was always monitored in order to detect any initial Pb in the analysed spots The observed ^{204}Pb signal intensities were <0.00001 V. The initial Pb may have originated from co-ablation of mineral/glass inclusions or contaminated Pb in cracks or on the sample surface. The isotope ratios of ^{207}Pb/^{206}Pb, ^{206}Pb/^{238}U ^{207}Pb/^{235}U, and ^{235}Th/^{238}U were calculated based on the measured isotope signals.

2.2.3. Data collection, reduction, and U-Pb age calculations

In this study, zircon/monazite was used as an external standard for U-Pb dating. Other standard zircons/monazites were treated as unknowns. Calibration against high quality age standards provides the best test for the ablation protocol. SRM 610 standard glass is also used as an external standard but is used only for tests of U-Pb elemental fractionation in different matrices. A standard and an unknown were each analysed, usually resulting in ten unknowns and eleven standard data points, respectively in one data set.

Each measurement consisted of two 30 s baseline measurements, followed by an idle time of 10 s with the laser on. 30 acquisition cycles were recorded with ~1 s or ~0.5 s time slices for 266 nm/50 µm/2–4 Hz or 266 nm/30 µm/2–10 Hz, and 200 nm/30 µm/5–25 Hz rotation raster craters, respectively. The 10 s idle time assures the stabilization of the 10^{12} Ω Faraday amplifiers.[19, 42, 45] No significant effect from the slow response time of the amplifiers[59] was observed with the hardware using a feedback circuit at the Faraday amplifier at the minimal response time (smallest Tau-factor setup) and with this protocol[19] partly due to the use of a large He-Ar mixing chamber (see **section 2.2.1**). The baseline signals were subtracted from the total signals for each

isotope peak. The net intensities (V) were used for isotope ratio calculations. As standard bracketing was used, no further mass-bias correction was made at this stage.

A dataset from each spot consisted of 30 isotope ratios of $^{206}Pb/^{238}U$ and $^{207}Pb/^{206}Pb$; $^{232}Th/^{238}U$ was analysed but not examined in this paper. An arithmetic mean and an error of 1SD were obtained for each run. The isotope ratios obtained in this way for the unknown from a single spot were then re-calculated using the reference isotope ratios of the standard by normalizing to two averaged sets of isotope ratios from the bracketing standard spots before and after the unknown. Error propagation between bracketing standards and bracketed unknowns were calculated by a Runge-Kutta method with a 95% confidence limit.[60] We then obtained $^{207}Pb/^{235}U$, $^{206}Pb/^{238}U$, and $^{207}Pb/^{206}Pb$ ages for each single spot of the unknown with a weighted mean and error. The weighted mean and error were calculated by the following equation: $x \pm \sigma = [\Sigma(xi/\sigma i)^2]^{1/2}[\Sigma\,(1/\sigma i)^2]^{-1/2} \pm [\Sigma\,(1/\sigma i)^2]^{-1/2}$.[61]

The error correlation between the isotope ratios using a common isotope were calculated for $^{207}Pb/^{235}U$ and $^{206}Pb/^{238}U$,[62], where ^{235}U was calculated from measured ^{238}U using natural abundances of these isotopes (0.72 / 97.2745).[63] Finally, a U-Pb concordia age[61] was calculated with all spot analyses data using Isoplot ver. 2.2.[64] The reference isotope ratios for 91500 zircon were $^{207}Pb/^{206}Pb = 0.07488$ and $^{206}Pb/^{238}U = 0.1792$.[49] Corresponding ratios for 44069 monazite were $^{207}Pb/^{206}Pb = 0.05532$ and $^{206}Pb/^{238}U = 0.06811$.[45]

3. Results and discussion

3.1. Downhole fractionation and optimal ablation conditions

Downhole fractionation was observed more clearly by MFC-ICP-MS than by single IC- or MIC-ICP-MS. The authors tested both single spot and rotation raster protocols for 60 s using a 200FsLA/30 µm/5 Hz.[10] The results showed almost no fractionation when observed by a MIC-ICP-MS. Unlike MIC-ICP-MS, we needed stronger signals for MFC-ICP-MS because of an inferior sensitivity, despite the enhanced sensitivity at the ion interface. Downhole fractionation was enhanced due to the high aspect ratio of deep craters.[4] We thus conducted spot analyses with a 193ExLA/50 µm/2 and 3 Hz for 30 s and a 266FsLA/50 µm/2, 3, and 5 Hz for 30 s, and with a rotation raster protocol with a 200FsLA/20 µm/25 Hz laser beam rastering along the circumference of a circle with a 7 µm radius for 15 s, which resulted in a 30 µm crater. Drilling depths were 10 and 15 µm with the 193ExLA and 10, 15 and 25 µm with the 266FsLA depending on the laser repetition rate, and 20 µm with the 200FsLA rotation raster (RR).

Our new observations confirmed strong downhole fractionation of 10–15% in $^{206}Pb/^{238}U$ with nanosecond 193ExLA/50 µm using 91500 zircon (normalized to the first isotope ratio to be unity; **Fig. 1a**).[2] The magnitude of fractionation depended on the aspect ratio of the crater as previously reported.[4] The 266FsLA results also showed downhole fractionation to a lesser extent 3–8% (**Fig. 1b**). However, again, a high aspect ratio was the source of elemental fractionation. The use of the 266FsLA/50 µm/2 Hz nearly eliminated downhole fractionation (<2%), and therefore was used in this setting. For comparison, we also use a spot crater with the 266FsLA/30 µm/10 Hz for 15 s, for which the extent of fractionation was almost identical (7%) to that of the 266FsLA/50 µm/5 Hz (**Fig. 1b**). A better result was obtained from the 200FsLA/30 µm RR protocol. Fractionation was less than 2% or negligible (**Fig. 1c**). Analyses of 91500 and NIST SRM610 glass showed almost no fractionation in 200FsLA/30 µm RR/25 Hz for 15 s.

This lack of fractionation is encouraging for a precise age determination, but elemental fractionation still existed between glass and zircon/monazite, preventing the use of a glass standard for U-Pb dating of zircon or monazite (see below **section 3.2**).

We mostly use a 266FsLA/50 µm/2 Hz (~10 µm depth, 30 s) and a 200FsLA/30 µm RR/25 Hz (~20 µm depth, 15 s) in the following experiments unless otherwise noted. The ablated sample volumes were ~1.96 and ~1.77 × 10^{-5} cm^3, respectively.

3.2. Matrix effect: glass versus zircon

A matrix matched standard is required for the accurate determination of elemental abundances[9] and U-Pb dating.[2] Fractionation occurs at the laser ablation site and in the ICP. The interrelation with the LA and ICP sites makes the true origins of this effect difficult to identify. We have tested the dating of 91500 zircon[49] using NIST SRM610 glass as a standard.[54] The $^{207}Pb/^{206}Pb$ isotope ratio of SRM610 glass was obtained from the literature ($^{207}Pb/^{206}Pb$ = 0.91006)[65] and the $^{206}Pb/^{238}U$ ratio was calculated based on the elemental abundances measured from a half-cut of the same SRM610 glass disk ($^{206}Pb/^{238}U$ = 0.26178). We used both the 266FsLA/50 µm/2 Hz spot crater and the 200FsLA/50 µm RR/25 Hz.

Measured $^{206}Pb/^{207}Pb$ ages were 1075.1 ± 8.5 Ma (266FsLA/50 µm/2 Hz) and 1068.8 ± 11.1 Ma (200FsLA/50 µm RR/25 Hz) weighted averages, showing a good match with the ID-TIMS age of 1065.4 ± 0.3 Ma.[49] In contrast, the averages for $^{206}Pb/^{238}U$ ages were 1139.4 ± 17.3 Ma and 1142.6 ± 16.2 Ma, corresponding to large differences from the ID-TIMS age of 1063.5 ± 0.6 Ma (**Fig. 2**).[49] The $^{206}Pb/^{238}U$ ratios measured in zircon are ~6% higher, indicating Pb enhancement in the zircon aerosol

relative to glass aerosol, irrespective of wavelength of laser light (200 vs. 266 nm) and ablation mode (spot vs. rotation raster).

Such a discrepancy may stem from the different ionization efficiency in the ICP caused by a different matrix, where more refractory metals Zr and Hf are dominant in the 91500 aerosols than in the Si-rich SRM 610 aerosols. The melting and boiling points of Si are 1683 K and 2628 K, respectively. Those of Zr are 2125 K and 4650 K.[66] The first ionization potential of Si is 300 kJ mol^{-1} and that of Zr is 700 kJ mol^{-1}.[66] The insufficient ionization of U (1405.5 K, 4018 K, 1120 kJ mol^{-1}) relative to Pb (600.65 K, 2013 K, 1080 kJ mol^{-1})[66] in the zircon matrix could originate from the relative suppression of U ionization in the Zr-rich refractory matrix. Dissociation of the laser particles with the refractory matrix (high melting and boiling points) can be slow due to the low thermal conductivity in the particles. Insufficient heating of particles may prevent the release of U relative to volatile Pb.[9, 17, 32]

The effective release of volatile Pb relative to refractory U can occur from the refractory zircon matrix by thermal effects.[3, 9, 32] To test the problem, the different laser wavelength and ablation protocol between the 266FsLA spot versus 200FsLA rotation raster tested in this study showed almost no downhole fractionation (see **Fig. 1b and c**). Furthermore, the extent of U-Pb fractionation is almost identical between the two protocols (**Fig. 2**). This suggests the crucial role of the ICP rather than the laser ablation site.[9, 17] In fact, laser aerosols generated by the 266FsLA and 200FsLA showed almost the same particle size distribution irrespective of different matrix between Si-rich SRM612 and Si-poor basalt glass BHVO-2G.[9] The observed elemental fractionation between these two samples was explained through the difference in the glass matrix, which had different thermal conductivities.[9] The source of the matrix effect is probably

the thermal conductivity (or bulk dissociation energy) of the laser aerosols controlled mainly by the constituent major element in the samples and this affected ionization efficiencies in the ICP.

3.3. Temporal variation of elemental and mass fractionations

The high efficiency ion interface used in this study yielded extremely large amounts of oxides particularly in U due to the high dissociation energy of UO^+ (**section 2.2**). The yield of U^+ ion can be suppressed by low oxide-yield interface settings.[10, 42] In this study, we gave the first priority to the sensitivity of Pb in order to achieve the best precision for U-Pb dating with the use of Faraday collectors. A study on the minimization of UO^+ and thus U-Pb fractionation is beyond the scope of this paper. However, features of elemental and mass bias fractionation should be examined with this extreme high-sensitivity and high-oxide yield setting (**Table 1**).

Temporal changes occur in elemental sensitivity between U and Pb (shown by $^{206}Pb/^{238}U$ in **Fig. 3a**). This also occurs in the mass bias of Pb isotopes (shown by normalized $^{207}Pb/^{206}Pb$ in **Fig. 3b**). These are most probably due to changes in the conditions at the ion interface. The UO^+ yield continuously decayed with time after the plasma was turned on, largely accounting for the continuous change in $^{206}Pb/^{238}U$ ratios. Tuning of the Ar sample gas flow and X–Y positions of the ICP torch caused an abrupt change in the decay profile, but the continuous decay did not stop (**Fig. 3a**). The change at the interface also affected the instrumental mass bias in Pb isotope ratios, showing a rapid decrease in $^{207}Pb/^{206}Pb$ in the first ~2 h (~0.01 per mass unit) and a flatter but continuous lowering afterwards (0.001 per mass unit; see **Fig. 3b**). This observation also indicates that the instability is from the ion interface rather than the torch or the

contaminated air in the laser cell. Pb isotopes are nearly unaffected by oxide yield. The profiles are almost identical between Day 1 and Day 2, as shown by the profiles of the 91500 standard (**Fig. 3a and 3b**).

A similar decay pattern has been reported in the Xe baseline, which decayed rapidly in the first ~2 h and readily stabilized but decreased continuously for up to ~6 h.[67] We do not explore the origin of these instabilities, which are beyond the scope of this paper. A future study of the possible origin of this instability may aid in the understanding of the ICP-MS instrument and analytical performance. For a practical solution, we used the frequent analyses of the bracketing standards 91500 zircon and 44069 monazite for high precision zircon/monazite U-Pb dating. As shown by the $^{206}Pb/^{238}U$ and $^{207}Pb/^{206}Pb$ relationship between the 91500 (standard) and the Prešovice and TEMORA2 (unknown) zircons, the use of alternating standard bracketing minimizes the elemental and isotopic fractionations in LA-MFC-ICP-MS. We apply this analytical protocol throughout this paper.

3.4. U-Pb dating of zircons

We analysed TEMORA2 (416.78 ± 0.33 Ma: ID-TIMS),[6] Prešovice (337.13 ± 0.37 Ma: ID-TIMS),[48] and OD-3 (33.0 ± 0.1 Ma: SHRIMP)[8] zircon using a 91500 zircon (1065.4 ± 0.6 Ma: ID-TIMS)[49] as the bracketing standard. We tested two ablation protocols using a 266FsLA/50 μm/2 Hz spot analysis (30 s) and 200FsLA/30 μm RR/25 Hz analysis (15 s). An additional 266FsLA/30 μm/10 Hz spot analysis (15 s) was also tested once on TEMORA2 (20140630). Summaries of $^{207}Pb/^{235}U$, $^{206}Pb/^{238}U$ and $^{207}Pb/^{206}Pb$ ages are shown in **Table 2**. The entire analytical results are given in **E.S.I. Data Table 1**.† Concordia plots are shown in **Fig. 4** (results of 20140630 not shown).

The obtained U-Pb concordia ages of TEMORA2 were 417.4 ± 1.8 Ma (266FsLA/50 μm/2 Hz) and 417.7 ± 2.1 Ma (200FsLA/30 μm RR/25 Hz) and 418.8 ± 3.9 Ma (266FsLA/30 μm/10 Hz, not shown) (**Fig. 4a and 4b**) consistent with 416.78 ± 0.33 Ma measured by ID-TIMS. Those for Prešovice were 336.5 ± 1.5 Ma (266FsLA/50 μm/2 Hz) and 334.6 ± 1.5 Ma (200FsLA/30 μm RR/25 Hz) for 337.13 ± 0.37 Ma measured by ID-TIMS. The young OD-3 zircon was dated as 33.29 ± 0.19 Ma (266FsLA/50 μm/4 Hz; repetition rate increased to 4 Hz due to low Pb) and as 32.86 ± 0.21 Ma (200FsLA/30 μm RR/25 Hz). Both ages compared quite well with the two SHRIMP ages of 32.96 ± 0.17 Ma and 32.91 ± 0.52 Ma.[8]

The internal age precisions from age errors were 0.43–0.5% for TEMORA2 and Prešovice and ~0.6% for OD-3. The reproducibility (absolute age offsets from the reference ID-TIMS or SHRIMP ages) were 0.15–0.22% for TEMORA2 and 0.2–0.7% for Prešovice, and 1.1 and 0.2% for OD-3 (**Table 2**). The range of internal age precisions and the intermediate age precisions were within comparable levels showing precise and accurate analyses. These levels were comparable with those obtained by SHRIMP.[6, 8, 48] The stability of this new technique was tested for well over six months with different samples, while skimmer cones and instrumental settings changed daily (See **E.S.I. Data Table 1**†).

3.5. U-Pb dating of monazites

Monazite is a rare earth element (REE)-U-Th phosphate and has also been used for U-Pb dating. Because of the very different matrix in comparison to zircon and glass, a monazite standard is required for U-Pb dating.[45, 50] We used 44069 monazite as the standard with the ID-TIMS age of 424.9 ± 0.4 Ma and SHRIMP $^{206}Pb/^{238}U$ ages within

418–438 Ma.[53] The monazites treated as unknowns were the Thompson Mine[50] and the Monangotry.[45, 52]

Monazite usually contains high U and Th concentrations, and so the radiogenic $^{206\text{-}208}$Pb concentration is also high. In order to adjust the upper current limits of the 10^{12} Ω amplifiers (< 3 V, where <1 V is set in practice in order to avoid amplifier current overload from sudden increase in laser signals), the repetition rate was lowed to 200FsLA/30 µm RR/5 Hz/15 s. The spot analysis was made with 266FsLA/30 µm/2 Hz/15 s for comparison. The resultant crater depths were ~5 µm, respectively, and the ablated sample volumes were ~0.35×10^{-5} cm^3 by both ablation protocols, about one fourth of the corresponding volume used for zircons. The sample volume was about 15 times smaller than that used in a previous attempt using LA-MFC-ICP-MS (~5.4×10^{-5} cm^3).[45] Ten spots were analysed by the two methods for both the Thompson Mine and Monangotry monazite samples. A 44069 monazite was analysed between the unknowns. Analytical results are summarized in **Table 3** and all the results are shown in **ESI Data Table 2**†.

The U-Pb age of the Thompson Mine monazite showed 1761 ± 4 Ma (266FsLA/30 µm/2 Hz) and 1755 ± 4 Ma (200FsLA/30 µm RR/5 Hz) (**Fig. 5a and 5b**). These ages were identical and consistent with the ID-TIMS age of 1766 Ma[50] within a 0.6–0.2% age offset. Ages for the Manangotry monazite were 560.8 ± 11 Ma (266FsLA/30 µm/2 Hz) and 562.4 ± 4.5 Ma (200FsLA/30 µm RR/5 Hz) (**Fig. 5c and 5d**), a 1.3–1.0% age offset from the ID-TIMS age of 555 ± 1.8 Ma[45] or a 0.7–0.5% age offset from 558 ± 3 Ma by LA-MFC-ICP-MS.[45] Discordant plots (the offset of the error ellipsoids beneath the U-Pb age concordia line) are similar to those reported by previous LA-MFC-ICP-MS measurements.[45] Internal precision (age errors) was within the levels

of those age offsets, indicating sufficient intermediate precision. The resulting U-Pb ages for the monazite varied significantly under the precision defined here. The origin of this discrepancy can be heterogeneity of the standard monazites.[11]

4. Conclusions

We present a new analytical technique for precise U-Pb dating of zircon and monazite crystals using 266/200FsLA-MFC-ICP-MS. This method provides accurate and precise age determination with a ~0.5% age error and the smaller age offset from ID-TIMS, which are comparable to those of SHRIMP. A high efficiency ion sampling interface in the MFC-ICP-MS combined with high gain amplifiers equipped with a 10^{12} Ω resistor enabled the use of Faraday collectors to determine $^{207}Pb/^{206}Pb$ and $^{206}Pb/^{238}U$ isotope ratios from laser craters as small as 30 µm×20 µm (diameter × depth) on the zircons and 30 µm×5 µm on the monazites. Optimization of laser ablation protocols using 266/200FsLA minimized downhole fractionation within 1–2% (1SD) for all isotope ratios of interest. All of these improvements made accurate U-Pb dating possible with this method. We presented analytical results of TEMORA2, Prešovice and OD-3 standard zircons, and the Thompson Mine and Monangotry monazites for applications of this technique. All the analytical results reproduced the reference ages within an age offset of 0.15–0.7% for ID-TIMS ages for zircons and 0.2–0.7% for monazites, clearly demonstrating the high precision of U-Pb age dating, although necessary sample volume for a single spot is still ten times greater than that for SHRIMP.

Acknowledgements

We thank Dr. Iwano H. and Dr. Danhara T. of Kyoto Fission–Track Co. Ltd. for discussions on data handling in the U-Pb age dating of zircon. Discussions with Dr. Bouman C. of Thermo Elemental were useful in the application of high gain amplifiers to this project. Comments from two anonymous reviewers were extremely useful and improved this manuscript.

References

1. T. Hirata and R. W. Nesbitt, *Geochimica et Cosmochimica Acta*, 1995, **59**, 2491-2500.
2. S. E. Jackson, N. J. Pearson, W. L. Griffin and E. A. Belousova, *Chemical Geology*, 2004, **211**, 47-69.
3. S. M. Eggins, L. P. J. Kinsley and J. M. G. Shelley, *Applied Surface Science*, 1998, **127-129**, 278-286.
4. I. Horn, R. L. Rudnick and W. F. McDonough, *Chemical Geology*, 2000, **164**, 281-301.
5. M. Tiepolo, *Chemical Geology*, 2003, **199**, 159-177.
6. L. P. Black, S. L. Kamoc, C. M. Allen, D. W. Davis, J. N. Aleinikoff, J. W. Valleye, R. Mundilf, I. H. Campbell, R. J. Korsch, I. S. Williams and C. Foudoulis, *Chemical Geology*, 2004, **205**, 115-140.
7. T. Hirata, Y. Hayano and T. Ohno, *Journal of Analytical Atomic Spectrometry*, 2003, **18**, 1283-1288. DOI: 10.1039/b305127g.
8. H. Iwano, Y. Orihashi, T. Hirata, M. Ogasawara, T. Danhara, K. Horie, N. Hasebe, S. Sueoka, A. Tamura, Y. Hayasaka, A. Katsube, H. Ito, K. Tani, J.-I. Kimura, Q. Chang, Y. Kouchi, Y. Haruta and K. Yamamoto, *Island Arc*, 2013, **22**, 382-394. DOI: 10.1111/iar.12038.
9. J.-I. Kimura and Q. Chang, *Journal of Analytical Atomic Spectrometry*, 2012, **27**, 1549-1559. DOI: 10.1039/c2ja10344c.
10. J.-I. Kimura, Q. Chang and K. Tani, *Geochemical Journal*, 2011, **45**, 283-296.
11. T. Iizuka and T. Hirata, *Geochemical Journal*, 2004, **38**, 229-241.
12. M. Guillong, I. Horn and D. Günther, *Journal of Analytical Atomic Spectrometry*, 2003, **18**, 1224-1230.

13. A. Cocherie, C. M. Fanning, P. Jezequel and M. Robert, *Geochimica et Cosmochimica Acta*, 2009, **73**, 1095-1108.
14. I. Horn and D. Günther, *Applied Surface Science*, 2003, **207**, 144-157.
15. C. Paton, J. D. Woodhead, J. C. Hellstrom, J. M. Hergt, A. Greig and R. Mass, *Geochemistry, Geophysics, Geosystems*, 2010, **11**, doi:10.1029/2009GC002618.
16. D. B. Aeschliman, S. J. Bajic, D. P. Baldwin and R. S. Houk, *Journal of Analytical Atomic Spectrometry*, 2003, **18**, 1008-1014.
17. I. Kroslakova and D. Günther, *Journal of Analytical Atomic Spectrometry*, 2007, **22**, 51-62.
18. A. Montaser, *Inductively Coupled Plasma Mass Spectrometry*, Wiley-VCH, New York. 1998.
19. J.-I. Kimura, H. Kawabata, Q. Chang, T. Miyazaki and T. Hanyu, *Geochemical Journal*, 2013, **47**, 369-384.
20. A. J. R. Kent and J. H. Dilles, *Geochimica et Cosmochimica Acta*, 2005, **69**, A376-A376.
21. C. M. Allen and I. H. Champbell, *Chemical Geology*, 2012, **332-333**, 157-165. DOI: 10.1016/j.chemgeo.2012.09.038.
22. P. Telouk, E. F. Rose-Koga and F. Albarède, *Geostandards Newsletter*, 2003, **27**, 5-11.
23. I. Horn and F. v. Blanckenburg, *Spectrochimica Acta*, 2007, **B62**, 410-422.
24. J. Koch, A. v. Bohlen, R. Hergenröder and K. Niemax, *Journal of Analytical Atomic Spectrometry*, 2004, **19**, 264-272.
25. J. Pisonero and D. Günther, *Mass Spectrometry Reviews*, 2008, **27**, 609-623.
26. J. Koch, M. Wälle, J. Pisonero and D. Günther, *Journal of Analytical Atomic Spectrometry*, 2006, **21**, 932-940.
27. C. C. Garcia, H.Lindner, A. v. Bohlen, C. Vadlab and K. Niemax, *Journal of Analytical Atomic Spectrometry*, 2008, **23**, 470-478.
28. F. Poitrasson, X. Mao, S. S. Mao, R. Freydier and R. E. Russo, *Analytical Chemistry*, 2003, **75**, 6184-6190.
29. F. Claverie, B. Fernández, C. Pécheyran, J. Alexis and O. F. X. Donard, *Journal of Analytical Atomic Spectrometry*, 2009, **24**, 891-902.
30. R. E. Russo, X. L. Mao, C. Liu and J. Gonzalez, *Journal of Analytical Atomic Spectrometry*, 2004, **19**, 1084-1089.
31. F.-X. D'Abzac, F. Poitrasson, R. Freydier and A.-M. Seydoux-Guillaume, *Journal of Analytical Atomic Spectrometry*, 2010, **15**, 681-689.
32. F.-X. D'Abzac, A.-M. Seydoux-Guillaume, J. Chmeleff, L. Datas and F.

Poitrasson, *Journal of Analytical Atomic Spectrometry*, 2011, DOI:10.1039/c1031ja10145d.

33. T. Hirata, *Analyst*, 1996, **121**, 1407-1411.

34. A. J. Walder, I. Platzne and P. A. Freedman, *Journal of Analytical Atomic Spectrometry*, 1993, **8**, 19-23.

35. A. Simonetti, L. M. Heaman, R. P. Hartlaub, R. A. Creaser, T. G. MacHattiea and C. Böhm, *Journal of Analytical Atomic Spectrometry*, 2005, **20**, 677-686.

36. J. M. Koornneef, C. Bouman, J. B. Schwieters and G. R. Davies, *Journal of Analytical Atomic Spectrometry*, 2013, **28**, 749-754.

37. J. M. Koornneef, C. Bouman, J. B. Schwieters and G. R. Davies, *Analytica Chimica Acta*, 2014, **819**, 49-55.

38. J.-I. Kimura, T. Nozaki, S. R. and K. Suzuki, *Journal of Analytical Atomic Spectrometry*, 2014, DOI: 10.1039/c1034ja00092g.

39. Q. Chang, J.-I. Kimura, T. Miyazaki, S. Sasaki and N. Kanazawa, *Geochemical Journal*, 2014, **48**, 309-320. DOI: 10.2343/geochemj.2.0307.

40. B. Paul, J. D. Woodhead and J. Hergt, *Journal of Analytical Atomic Spectrometry*, 2005, **20**, 1350-1357. DOI: 10.1039/b507647a.

41. B. Paul, J. D. Woodhead, J. Hergt, L. Danyushevsky, T. Kunihiro and E. Nakamura, *Chemical Geology*, 2011, **289**, 210-223. DOI: 10.1016/j.chemgeo.2011.08.005.

42. J.-I. Kimura, Q. Chang and H. Kawabata, *Journal of Analytical Atomic Spectrometry*, 2013, **28**, 1522-1529. DOI: 10.1039/c3ja50109d.

43. J.-I. Kimura, T. Takahashi and Q. Chang, *Journal of Analytical Atomic Spectrometry*, 2013, **28**, 945-957. DOI: 10.1039/c3ja30329b.

44. J.-I. Kimura, K. Tani and Q. Chang, *Geochemical Journal*, 2012, **46**, 1-12.

45. M. S. A. Horstwood, G. L. Foster, R. R. Parrish, S. R. Noble and G. M. Nowell, *Journal of Analytical Atomic Spectrometry*, 2003, **18**, 837-846. DOI: 10.1039/b304365g.

46. C. Bouman, M. Deerberg, J. B. Schwieters and T. F. Scientific, *Application Note of Thermo Fischer Scientific*, 2008, **30187**, 1-4.

47. L. P. Black, S. L. Kamo, C. M. Allen, J. N. Aleinikoff, D. W. Davis, R. J. Korsch and C. Foudoulis, *Chemical Geology*, 2003, **200**, 155-170.

48. J. Slama, J. Kosler, D. J. Condon, J. L. Crowley, A. Gerdes, J. M. Hanchar, M. S. A. Horstwood, G. A. Morris, L. Nasdala, N. Norberg, U. Schaltegger, B. Schoene, M. N. Tubrett and M. J. Whitehouse, *Chemical Geology*, 2008, **249**, 1-35. DOI: 10.1016/j.chemgeo.2007.11.005.

49. M. Wiedenbeck, P. Alle, F. Corfu, W. L. Griffin, M. Meier, F. Oberli, A. v. Quadt, J. C. Roddick and W. Spiegel, *Geostandards Newsletter*, 1995, **19**, 1–24.

50. I. S. Williams, I. S. Buick and I. Cartwright, *Journal of Metamorphic Geology*, 1996, **14**, 29-47.

51. J. Taylor, G. Stevens, I. S. Buick and C. Lana, *Geological Society of America Bulletin*, 2012, **124**, 1191-1211. DOI: 10.1130/B30543.1.

52. J.-L. Paquette, A. Nedelec, B. Moine and M. Rakotondrazafy, *The Journal of Geology*, 1994, **102**, 523-538.

53. J. N. Aleinikoff, W. S. Schenck, M. O. Plank, L. Srogi, C. M. Fanning, S. L. Kamo and H. Bosbyshell, *Geological Society of America Bulletin*, 2006, **118**, 39-64. DOI: 10.1130/B25659.1.

54. K. P. Jochum, U. Nohl, K. Herwig, E. Lammel, B. Stoll and A. W. Hofmann, *Geostandards and Geoanalytical Research*, 2005, **29**, 333-338.

55. J.-I. Kimura, K. Tani and Q. Chang, *Geochemical Journal*, 2012, **46**, 1-12.

56. K. Newman, *Journal of Analytical Atomic Spectrometry*, 2011, **27**, 63-70. DOI: 10.1039/c1ja10222b.

57. K. Newman, P. A. Freedman, J. Williams, N. S. Belshaw and A. N. Halliday, *Journal of Analytical Atomic Spectrometry*, 2009, **24**, 742-751. DOI: 10.1039/b819065h.

58. B. D. Darwent, *National Standard Reference Series, National Bureau of Standards US*, 1970, **NSRDS-NBS 31**, 1-48.

59. T. Hirata, Y. Hayano and T. Ohno, *Journal of Analytical Atomic Spectrometry* 2003, **18**, 1283-1288.

60. J. Kragen, *Analyst*, 1994, **119**, 2161-2165.

61. G. Faure, *Principles of Isotope Geology*, John Wiley & Sons, New York. 1977.

62. M. D. Schmitz and B. Schoene, *Geochemistry, Geophysics, Geosystems*, 2007, **8**, DOI:10.1029/2006GC001492.

63. International_Union_of_Pure_and_Applied_Chemistry, *Pure & Applied Chemistry*, 1984, **56**, 695-768.

64. K. R. Ludwig, *Berkeley Geochronology Center, Special Publication*, 2001, **1a**, 53 pp.

65. J. D. Woodhead and J. M. Hergt, *Geostandards Newsletter: The Journal of Geostandards and Geoanalysis*, 2001, **25**, 261-266.

66. J. Emsley, *The Elements*, Clarendon Press, Oxford. 1998.

67. T. Miyazaki, J.-I. Kimura and Q. Chang, *Journal of Analytical Atomic Spectrometry*, 2014, **29**, 483-490. DOI: 10.1039/c3ja50311a.

Figure captions

Fig. 1 Downhole fractionation profiles of $^{206}Pb/^{238}U$ ratios from 91500 zircon and photomicrographs of the laser ablation craters. Abscissa are scan numbers in 30 s for panels a and b, and in 15 s for panel c. 193ExLA shows strong fractionation even in the first 15 s. Minimized fractionation is achievable by 50 µm/2 Hz by 266FsLA and 30 µm RR/20 Hz by 200FsLA. Data are normalized to the first isotope ratio in the same run. 193ExLA: 193 nm excimer laser ablation; 266FsLA: 266 nm femtosecond laser ablation; 200FsLA: 200 nm femtosecond laser ablation; RR: rotation raster ablation protocol. Insets are reflected light photomicrographs of the craters. Shorter time interval is used for 200FsLA in order to use flat signal region with a high repetition rate (20 Hz) ablation, which is needed for sufficient signal intensities in high precision U-Pb dating.

Fig. 2 Plots of $^{207}Pb/^{206}Pb$ and $^{235}U/^{206}Pb$ ages obtained from 91500 zircon determined by SRM610 glass as the standard using 266FsLA/50 µm/2 Hz (panel a) and 200FsLA/30 µm RR/25 Hz (panel b). $^{207}Pb/^{206}Pb$ ages reproduce the ID-TIMS age but $^{235}U/^{206}Pb$ ages are 6–7% older, reflecting the enhanced ^{206}Pb concentration in the SRM610 analyses. Calculations were made with IsoPlot v2.2.[64] Thick lines are U-Pb concordia age lines.[61]

Fig. 3 Temporal changes in $^{206}Pb/^{238}U$ and $^{207}Pb/^{206}Pb$ over ~5 h. Data were obtained by analysing 91500, Prešovice and TEMORA2 zircons. Tuning of the Ar sample gas and X–Y positions of the ICP torch were made at ~2 h after turning the plasma on. The results clearly show both elemental fractionation ($^{206}Pb/^{238}U$) and mass bias fractionation ($^{207}Pb/^{206}Pb$). Note that ablation conditions changed from 266FsLA/50

µm/2 Hz to 200FsLA/30 µm RR/25 Hz at ~2 h on Day 1. Fractionations are independent of the ablation method but depend of the tuning and interface conditions, which gradually change with time.

Fig. 4 Concordia plots of U-Pb age dating for TEMOTA2 (panels a and b), Prešovice (panels c and d), and OD-3 (panels e and f) zircons using 91500 zircon as an external standard. The left row was analysed by 266FsLA/50 µm/2–4 Hz whereas the right row was analysed using 200FsLA/30 µm RR/25 Hz. OD-3 zircons results are shown by Tera-Wasserburg plots for young zircons for which $^{238}U/^{206}Pb$ is more sensitive in age determination. All but panel e show concordia ages. Determined mean ages are comparable to those found by ID-TIMS and SHRIMP for TEMOTA2[6] and Prešovice,[48] and SHRIMP ages for OD-3.[8] Age calculations were conducted using IsoPlot v2.2.[64]

Fig. 5 Concordia plots of U-Pb age dating for Thompson Mine (panels a and b) and Monangotry (panels c and d) monazites. The left row was analysed by 266FsLA/30 µm/2 Hz, whereas the right row was analysed with 200FsLA/30 µm RR/2 Hz. Mean ages are comparable to those measured from ID-TIMS[50] and LA-ICP-MS,[45] for Thompson and ID-TIMS[45] and LA-MFC-ICP-MS[45] for Manangotry. The standard monazite 44069 was measured, with an ID-TIMS age of 424.9 ± 0.4 Ma and a SHRIMP age of 418–438 Ma.[53] Insets are reflected light photomicrographs of laser craters. Slightly larger craters are formed by a rotation raster protocol. Age calculations were made by IsoPlot v2.2.[64]

Table 1 Instrumental setup of lasers and MFC-ICP-MS

Table 2 Analytical results for the zircon U-Pb age

Table 3 Analytical results for the monazite U-Pb age

ESI Data Table 1: Analytical results for the U-Pb age of zircon crystals

ESI Data Table 2: Analytical results for the U-Pb age of monazite crystals

Tables Contents Entry: High precision U-Pb dating using multiple Faraday collectors has become available in LA-MC-ICP-MS

Table 1 Instrumental setup of lasers and MFC-ICP-MS

Femtosecond laser	OK Fs-2000K (OK Laboratory, in-house development)	
Laser source	800 nm near infrared T-sapphire one box regenerative amplifier (Spectra Physics, Solstice)	
Wave length	266 nm (frequency tripled by Spectra Physics, TP-1A THG)	
	200 nm (frequency quadrupuled by Spectra Physics, TP-1A FHG)	
Pulse width	< 300 fs for 200 nm and < 170 fs for 266 nm	
Pulse energy	> 300 μJ for 266 nm at laser output	
	> 60 μJ for 200 nm at laser output	
	> 150 μJ for 266 nm at sample surface	
	> 30 μJ for 200 nm at sample surface	
Focusing objective lens	THORLABS LMU-UV-193 objective lens for 200 nm	
	Edmund Optics single aspherical objective lens for 266 nm	
Beam diameter	5, 10, 15, 20, 25, 30 μm for 200 nm	
	15, 30, 40, 50, 60, 80 μm for 266 nm	
Repetition rate	2–25 Hz (see text)	
Laser fluence	~6 J cm^{-2} for 200 nm and ~12 J cm^{-2} for 266 nm	
Excimer laser	OK EX-2000 (OK Laboratory, in-house development)	
Laser source	193 nm/20 ns	
	ComPex102 (Coherent)	
Pulse width	20 ns	
Pulse energy	200 mJ	
Focusing objective lens	Imaging optics using field lens and air spaced doublet objective	
Beam diameter	30, 50, 100, 200 μm diameter	
Repetition rate	2 and 3 Hz	
Laser fluence	5-15 J cm^{-2}	
MFC-ICP-MS	Netpune (Thermo Scientific) modified	
RF-power	1500 W	
Guard electrode	On	
Sampling cone	JET-sample cone (Ni)	
Skimmer cone	X-skimmer cone (Ni)	
Cool gas (Ar)	13 L/min	
Auxiliary gas (Ar)	1.0 L/min	
Sample gas (Ar)	1.3 L/min	
Laser carrier gas (He)	1.15 L/min	
Interface vacuum with E2M80	1.8 mbar with He ablation career gas	
Mass resolution	Low resolution	
Acquisition time	1 s × 30 scans or 0.5 s × 30 scans	
Dispersion Quad	19.9 ($^{219.58}$M centre mass with zoom optics)	
Focus Quad	4–7	
Cup and amplifier configurations		
^{204}Pb	FC L4	10^{12} Ω resistor amplifier
^{206}Pb	FC L3	10^{12} Ω resistor amplifier
^{207}Pb	FC L2	10^{12} Ω resistor amplifier
^{208}Pb	FC L1	10^{12} Ω resistor amplifier
$^{219.58}$M	FC Axial	10^{11} Ω resistor amplifier (not observed in data acquisition)
^{232}Th	FC H2	10^{11} Ω resistor amplifier
^{238}U	FC H4	10^{12} Ω resistor amplifier
Background subtraction		On-peak background

FC: Faraday cup; isobaric atomic and molecular ions are shown in parentheses.

Table 2 Analytical results for the zircon U-Pb age

Date	Standard	Sample	Conditions	No.	$^{207}Pb/^{235}U$	Error	$^{206}Pb/^{238}U$	Error	$^{207}Pb/^{206}Pb$	Error	Conc. age	Error	Diff.%
TEMORA2			Dia./Rep./WL.		(Age Ma)								
20140620	91500	TEMORA2	50 μm/ 2 Hz/266 nm	n = 38	418.7	5.6	417.0	3.9	423.5	2.3	417.4	1.8	-0.15
20140630	91500	TEMORA2	30 μm/10 Hz/266 nm	n = 20	420.0	11.7	418.5	8.5	425.4	4.5	418.8	3.9	-0.48
20140708	91500	TEMORA2	30 μm RR/25 Hz/200 nm	n = 20	418.5	7.5	417.6	4.5	420.7	4.0	417.7	2.1	-0.22
Reference age: 416.78 ± 0.33 Ma (ID-TIMS), Black et al. (2004)													
Prešovice													
20140630	91500	Prešovice	50 μm/2 Hz/266 nm	n = 25	336.4	4.3	336.9	3.3	331.4	1.5	336.5	1.5	0.19
20140711	91500	Prešovice	30 μm RR/25 Hz/200 nm	n = 30	334.5	4.1	334.7	3.2	333.1	1.5	334.6	1.5	0.75
Reference age: 337.13 ± 0.37 Ma (ID-TIMS), Black et al. (2005)													
OD-3													
20140630	91500	OD-3	50 μm/4 Hz/266 nm	n = 25	38.9	1.7	33.3	0.4	345.1	14.0	33.29	0.19	-1.08
20140711	91500	OD-3	30 μm RR/25 Hz/200 nm	n = 15	34.1	1.9	32.9	0.4	108.5	5.7	32.86	0.21	0.23
Reference age: 33.0 ± 0.1 Ma (average of SHRIMP and LA-ICP-MS); Iwano et al. (2013)													

Note: Dia.: diameter; Rep.: repetition rate; WL.: wavelength, 1SD: 1-standard deviation; 2SD: 2-standard deviation; bold face: weighted average and error; Ma: million years ago; Diff.%: percentage difference of age from the reference value; Conc. Age: concordia age.

Decay constant used for the age calculations were 9.8485×10^{-10} yr^{-1} for ^{235}U and 1.55125×10^{-10} yr^{-1} for ^{238}U.

Weighted mean was calculated by the following equation: $x \pm \sigma = [\Sigma(xi/\sigma i)^2]^{1/2}[\Sigma\,(1/\sigma i)^2]^{-1/2} \pm [\Sigma\,(1/\sigma i)^2]^{-1/2}$.

Table 3 Analytical results for the monazite U-Pb age

Date	Standard	Sample	Conditions	No.	$^{207}Pb/^{235}U$	Error	$^{206}Pb/^{238}U$	Error	$^{207}Pb/^{206}Pb$	Error	Conc. Age	Error	Diff.%
Manangotry			Dia./Rep./WL.		(Age Ma)								
20140716	44069	Thompson	30 μm RR/5 Hz/200 nm	n = 10	1749	123	1744	57	1756	6	1755	4	-0.6
20140716	44069	Thompson	30 μm/2 Hz/266 nm	n = 10	1760	99	1759	45	1761	5	1761	4	-0.3
Reference age: 1766 Ma (ID-TIMS), Williams et al. (1996)													
20140716	44069	Manangotry	30 μm RR/5 Hz/200 nm	n = 10	551.4	20.2	546.4	15.7	572.1	2.8	562.4	4.5	0.8
20140716	44069	Manangotry	30 μm/2 Hz/266 nm	n = 10	546.5	16.2	537.7	12.2	578.2	2.5	560.8	11.0	0.5
Reference age: 558 ± 3Ma (LA-MFC-ICP-MS), Horstwood et al. (2003)													

Note: Dia.: diameter; Rep.: repetition rate; WL.: wavelength, 1SD: 1-standard deviation; 2SD: 2-standard deviation; bold face: weighted average and error; Ma: million years ago; Diff.%: percentage difference of age from the reference value; Conc. Age: concordia age.

Decay constant used for the age calculations were 9.8485×10^{-10} yr^{-1} for ^{235}U and 1.55125×10^{-10} yr^{-1} for ^{238}U.

Weighted mean was calculated by the following equation: $x \pm \sigma = [\Sigma(xi/\sigma i)^2]^{1/2}[\Sigma\ (1/\sigma i)^2]^{-1/2} \pm [\Sigma\ (1/\sigma i)^2]^{-1/2}$.

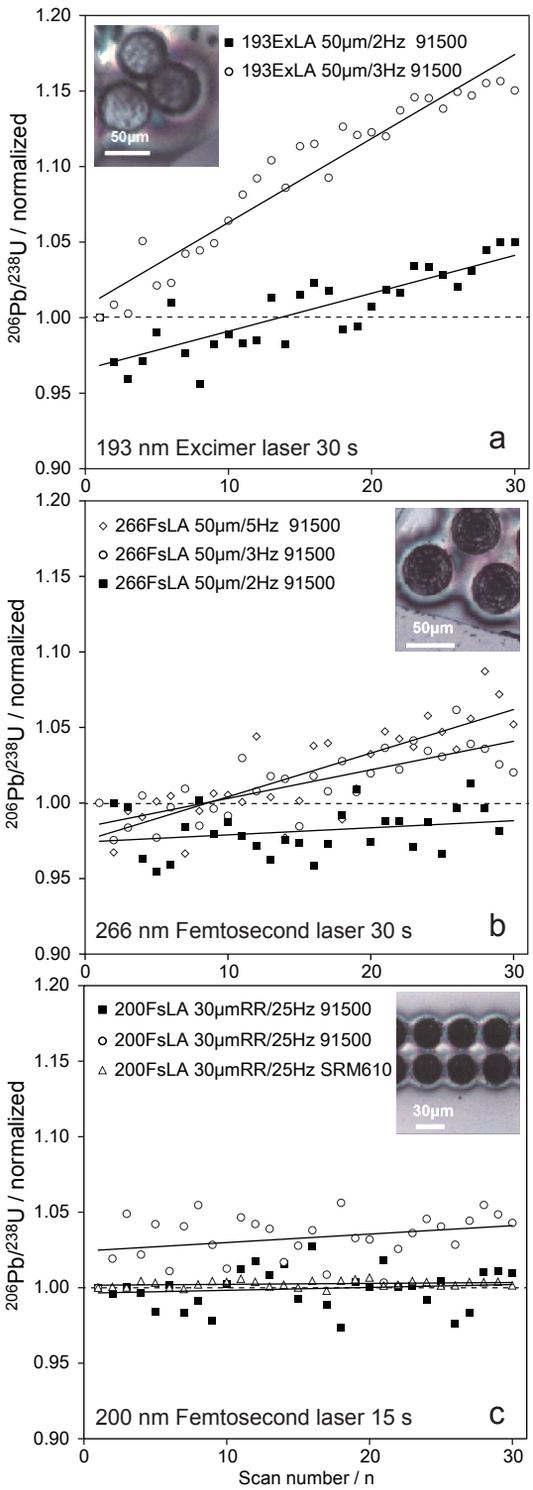

Fig. 1

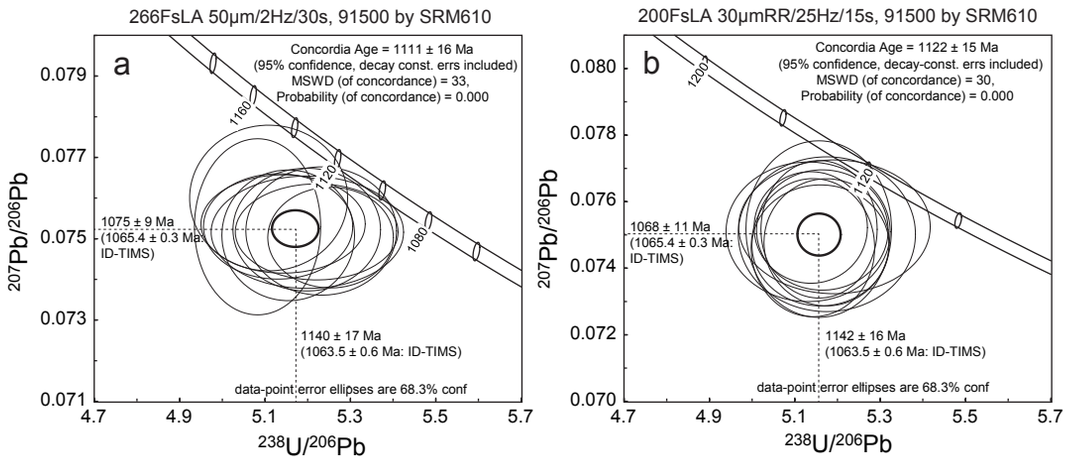

Fig. 2

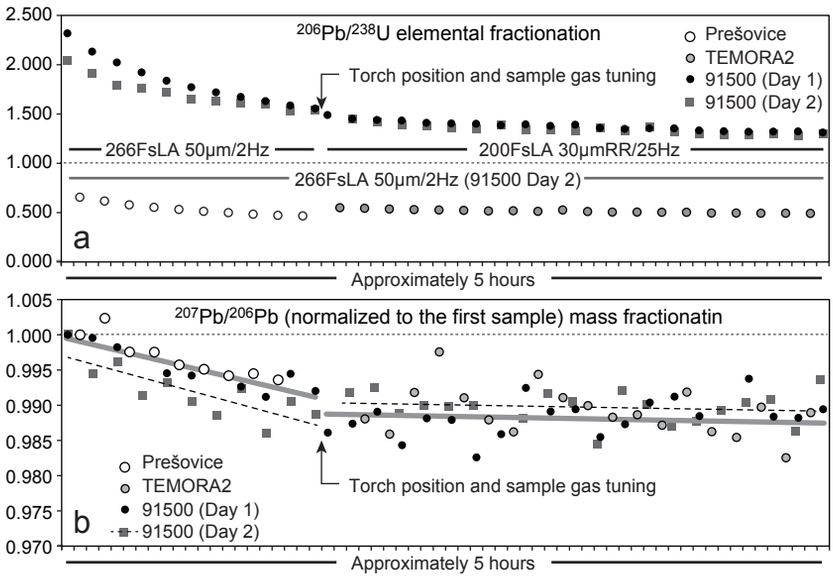

Fig. 3

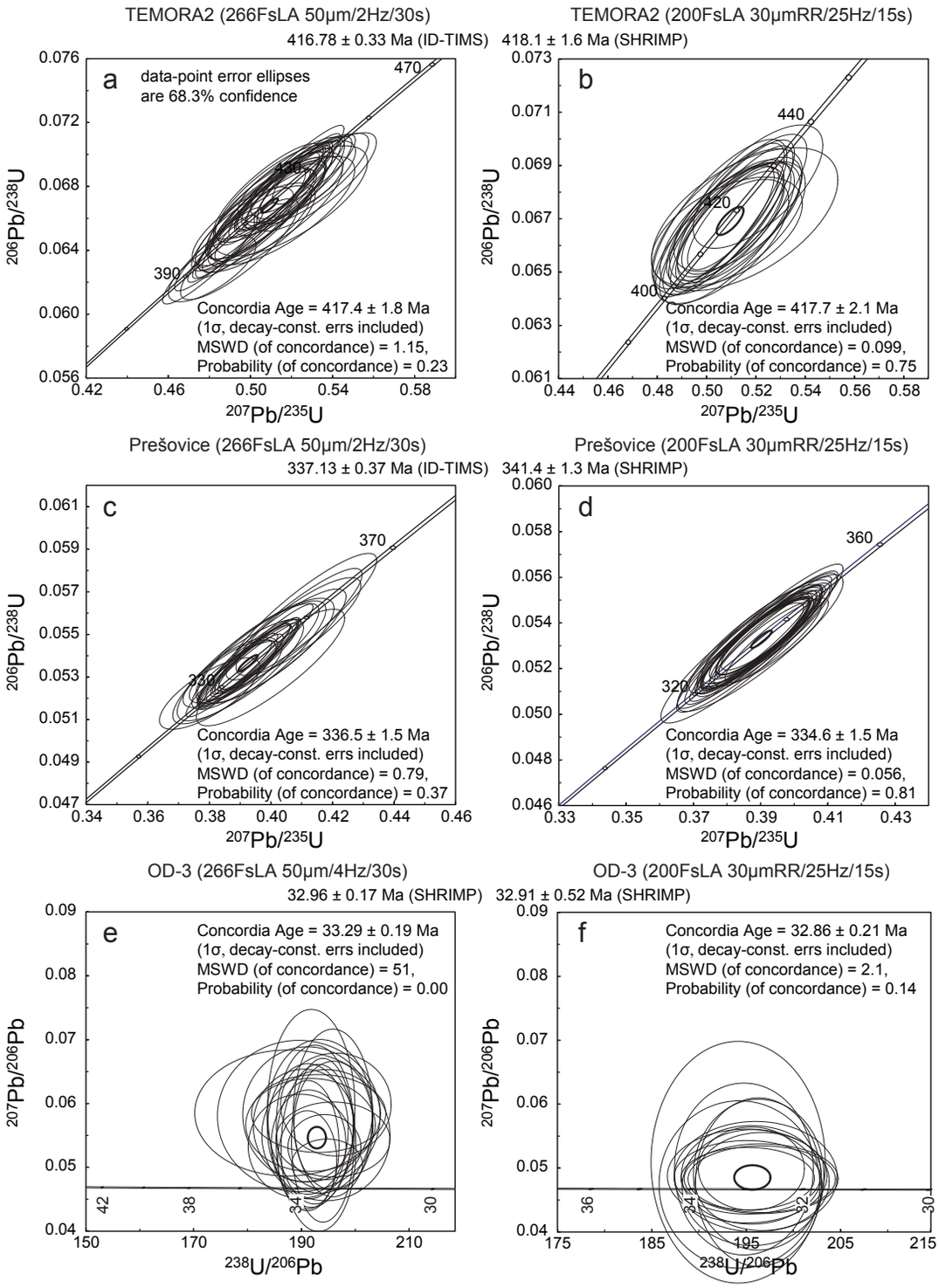

Fig. 4

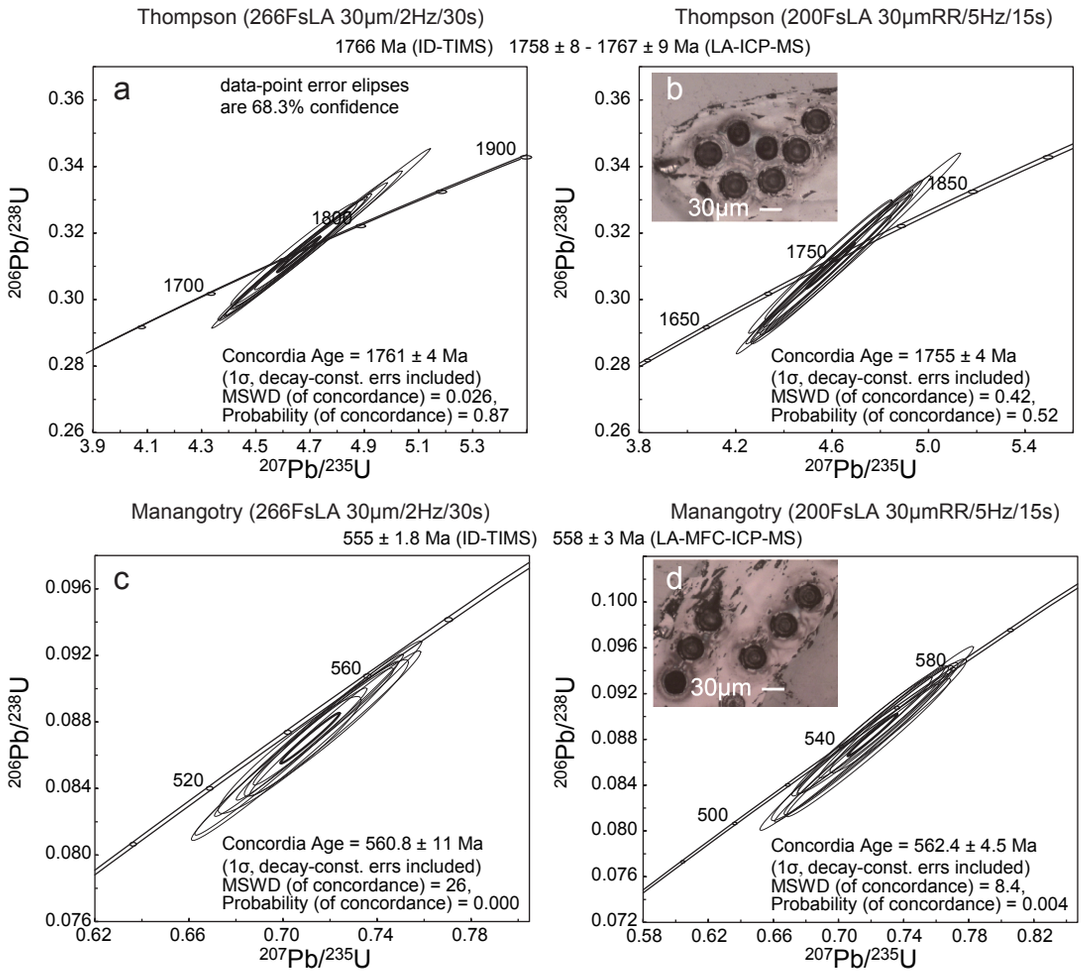

Fig. 5

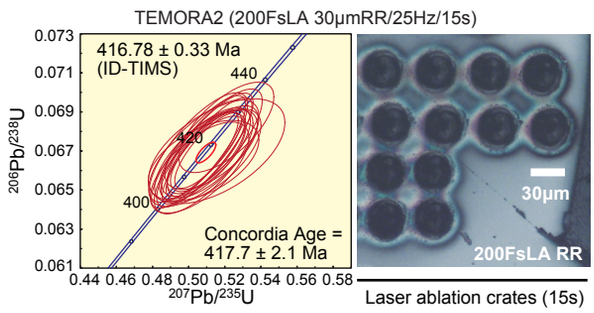

High precision U-Pb dating using multiple Faraday collectors has become available in LA-MC-ICP-MS